Contents lists available at ScienceDirect

Pharmacological Research

journal homepage: www.elsevier.com

Improvement of fiber connectivity and functional recovery after stroke by montelukast, an available and safe anti-asthmatic drug

Paolo Gelosa [a], Elisabetta Bonfanti [b], Laura Castiglioni [b], José Maria Delgado-Garcia [c], Agnès Gruart [c], Lucia Fontana [a, 1], Marco Gotti [a, 2], Elena Tremoli [a], Davide Lecca [b], Marta Fumagalli [b], Mauro Cimino [d], Ludwig Aigner [e], Maria P. Abbracchio [b], Luigi Sironi [a, b, *]

[a] Centro Cardiologico Monzino IRCCS, 20138 Milan, Italy
[b] Department of Pharmacological and Biomolecular Sciences, University of Milan, 20133 Milan, Italy
[c] Division of Neurosciences, Pablo de Olavide University, 41013 Seville, Spain
[d] Department of Biomolecular Sciences, University of Urbino, 61029 Urbino, Italy
[e] Institute of Molecular Regenerative Medicine, Spinal Cord Injury and Tissue Regeneration Center Salzburg, Paracelsus Medical University, 5020 Salzburg, Austria

ARTICLE INFO

Keywords:
Stroke
Montelukast (MTK)
Oligodendrocyte precursor cells (OPCs)
MRI fiber tracking
Electrophysiological recording

ABSTRACT

Stroke is one of the main causes of death, neurological dysfunctions or disability in elderly. Neuroprotective drugs have been proposed to improve long-term recovery after stroke, but failed to reach clinical effectiveness. Hence, recent studies suggested that restorative therapies should combine neuroprotection and remyelination. Montelukast, an anti-asthmatic drug, was shown to exert neuroprotection in animal models of CNS injuries, but its ability to affect oligodendrocytes, restoring fiber connectivity, remains to be determined.

In this study, we evaluated whether montelukast induces long-term repair by promoting fiber connectivity up to 8 weeks after middle cerebral artery occlusion (MCAo), using different experimental approaches such as *in vivo* diffusion magnetic resonance imaging (MRI), electrophysiological techniques, *ex vivo* diffusion tensor imaging (DTI)-based fiber tracking and immunohistochemistry. We found that, in parallel with a reduced evolution of ischemic lesion and atrophy, montelukast increased the DTI-derived axial diffusivity and number of myelin fibers, the density of myelin binding protein (MBP) and the number of $GSTpi^{+}$ mature oligodendrocytes. Together with the rescue of MCAo-induced impairments of local field potentials in ischemic cortex, the data suggest that montelukast may improve fibers reorganization.

Thus, to ascertain whether this effect involved changes of oligodendrocyte precursor cells (OPCs) activation and maturation, we used the reporter GPR17iCreERT2:CAG-eGreen florescent protein (GFP) mice that allowed us to trace the fate of OPCs throughout animal's life. Our results showed that montelukast enhanced the OPC recruitment and proliferation at acute phase, and increased their differentiation to mature oligodendrocytes at chronic phase after MCAo.

Considering the crosstalk between OPCs and microglia has been widely reported in the context of demyelinating insults, we also assessed microglia activation. We observed that montelukast influenced the phenotype of microglial cells, increasing the number of M2 polarized microglia/macrophages, over the M1 phenotype, at acute phase after MCAo.

In conclusion, we demonstrated that montelukast improves fiber re-organization and long-term functional recovery after brain ischemia, enhancing recruitment and maturation of OPCs. The present data suggest that montelukast, an already approved drug, could be "repositioned "as a protective drug in stroke acting also on fiber re-organization.

* Corresponding author at: Department of Pharmacological and Biomolecular Sciences, University of Milan, Via G. Balzaretti 9, 20133 Milan, Italy.
Email address: luigi.sironi@unimi.it (L. Sironi)
[1] Present address: Neuroradiology Unit and Neuro Center, Humanitas Clinical and Research Center, Rozzano, Milan, Italy.
[2] Present address: Department of Pharmacological and Biomolecular Sciences, University of Milan, 20133 Milan, Italy.

https://doi.org/10.1016/j.phrs.2019.02.025
Received 16 July 2018; Received in revised form 1 February 2019; Accepted 23 February 2019
Available online xxx

1. Introduction

Every year approximately 15 million people worldwide suffer a stroke [1]. Although the option of thrombolysis and improved neurointensive care have strongly reduced death rate, stroke remains the second leading cause of disability after dementia. A rather neglected issue is the fact that secondary brain injury evolves for weeks after stroke [2] and no drugs are currently available to counteract stroke secondary events, including inflammation that leads to neuronal death and delayed neuro-regeneration [3]. While contributing to functional disability, this secondary long- term injury offers a wider "therapeutic window" for intervention compared to acute treatments.

In this respect, new opportunities derive from the "repurposing" of already marketed drugs displaying neuroprotective, and regenerative activities [4,5]. Of interest, the anti-asthmatic drug montelukast, an antagonist of CysLT receptor 1 (CysLTR-1), is a likely candidate for stroke treatment, since, among other pleiotropic beneficial effects, it contrasts the detrimental effects of cysteinyl-leukotrienes (CysLTs), potent pro-inflammatory mediators, that sharply increase in the early phase after the ischemic insult [6] and contribute to blood-brain barrier dysfunction and chronic damage progression [7,8]. Montelukast is effective against acute brain ischemia in rodents [9–11] and, recently, a study on a cohort of patients provided a first indication of montelukast for the secondary prevention of cardiovascular diseases, including stroke [12]. Moreover, montelukast increases neurogenesis and restores cognitive function in old animals [13].

Recent studies have demonstrated that, besides neuroprotective approaches that directly target neurons, neurological improvement could also be achieved by strategies that favour the recovery of oligodendrocytes, the myelin-forming cells, and thus counteract myelin loss [14]. The involvement of oligodendrocytes is of relevance, since stroke patients with white matter damage and demyelination typically show poor prognosis [15]. This is further supported by evidence that, in experimental stroke, strategies aimed at promoting post-injury remyelination [16] provide recovery through regaining of fast electrical conductivity and/or trophic support to neurons [17]. Recent evidence indicates a negative role of inflammation in define the oligodendrocyte survival and maturation in experimental models of CNS diseases [18,19]. Thus, the block of CysLTs-mediated inflammation by montelukast could favour oligodendrocytes protection. Furthermore, montelukast could promote whiter matter repair in a CysLTR-1 independent way by inhibiting the receptor GPR17 [9] which is expressed in OPCs and growing evidence indicate to be engaged in remyelinization [20,21] However, up to now, the involvement of montelukast in oligodendrocytes and white matter protection remains to be elucidated.

In our study, to prevent the acute and chronic activation [6] of the unfavourable inflammatory cascade provided by overproduction of CysLTs, we decided to treat animals before and after the ischemic induction. In animals undergoing middle cerebral artery occlusion (MCAo), we evaluated the long-term effect of montelukast treatment on cerebral damage and fiber re-organization using magnetic resonance imaging (MRI). In this context, we investigated the effect of montelukast on the recovery of electrophysiological parameters focusing on the involvement of oligodendrocytes as a yet unexplored target for the neuro-reparative mechanisms in stroke. Finally, to evaluate oligodendrogenesis and OPCs maturation, we took advantage of the reporter GPR17iCreERT2:CAG-eGreen Fluorescent Protein (GFP) mice [22].

2. Material and methods

2.1. Animals and experimental protocols

The procedures concerning animal care, surgery and euthanasia were carried out in accordance with Italian and Spanish laws and with the current European Union Council (2010/63/UE) guidelines for the use of laboratory animals in chronic studies. The experiments of *in vivo* MRI and of fate mapping using the conditional reporter GPR17-iCreERT2:CAG-eGFP mouse line were approved and authorized by the National Ministry of Health-University of Milan Committee (Approval number 12/12-30012012 and 479/2015-PR), while the electrophysiological experiments were approved by the Ethics Committee (2011/01/11) of the Pablo de Olavide University. The study was conducted applying the ARRIVE guidelines.

In this study, we used 8–9 week-old CD1 (n = 46; *protocols 1 and 2*) and 11 week-old GPR17-iCreERT2:CAG-eGFP report male mice (n = 40; *protocol 3*) that were randomly assigned to the experimental procedures by an independent person not involved in data acquisition and analysis. All the experiments were conducted in the light phase. After being intraperitoneally (i.p.) anesthetized with ketamine (100 mg/kg) and xylazine (20 mg/kg), mice were allocated to permanent middle cerebral artery occlusion (MCAo) or sham surgery, as previously described [23]. Operation time per animal did not exceed 15 min, during which the body temperature was continuously monitored and maintained at 37 ± 0.5 °C until awakening. The mice with subarachnoidal or intracerebral haemorrhage and MCAo-mice with a volume of the cortical ischemic lesion less than 10 mm^3 at 2 h were withdrawn from the study, in particular four CD1 mice and three GPR17-iCreERT2:CAG-eGFP mice.

Starting form 3 days before MCAo, mice were treated i.p. with vehicle or montelukast sodium powder (Cayman Chemical, Ann Arbor, MI, United States), dissolved as previously described [13], at a dose of 5 mg/kg/day for 6 days and then at a dose of 1 mg/kg/day [24] until sacrifice. A group of sham-operated mice was treated with vehicle and used as control. Mice were randomized into three different experimental protocols as follows (Fig. 1).

Finally, the mice were sacrificed at different time points after being anesthetized by an i.p. injection of ketamine (100 mg/kg) and xylazine (20 mg/kg).

Protocol 1 (Fig. 1A). The effects of MTK treatment on ischemic injury in the acute phase (up to 48 h) and on cerebral atrophy in the chronic phase (up to 8 weeks) were monitored by *in-vivo* MRI analysis into MCAo-Montelukast (n = 10) and MCAo-Vehicle (n = 11) CD1 mice.

One mouse for MCAo-Montelukast group and 2 mice for MCAo-Vehicle died within 1 week after surgery. At week 8, mice (MCAo-Montelukast, n = 9 and MCAo-Vehicle, n = 9) were euthanized and brain collected for immunofluorescence (n = 5 for each group) or for *ex-vivo* MRI analysis (n = 4 for each group) in order to get information on fiber reorganization.

Protocol 2 (Fig. 1B). The effects of MTK treatment on fiber connectivity were evaluated by local field potentials recording. Three weeks before surgery for MCAo or sham-operation, CD1 mice (n = 21) were implanted with two recording electrodes (as reported below). Two mice died after implantation. One week after electrodes implantation, the MCAo mice were assigned to MCAo-Montelukast (n = 8), MCAo-Vehicle (n = 7) and Sham-Vehicle (n = 4) groups. One MCAo-Vehicle mouse died after surgery. At week 8, mice were euthanized and brain collected for immunofluorescence (n = 5 for MCAo-Vehicle and MCAo-Montelukast groups).

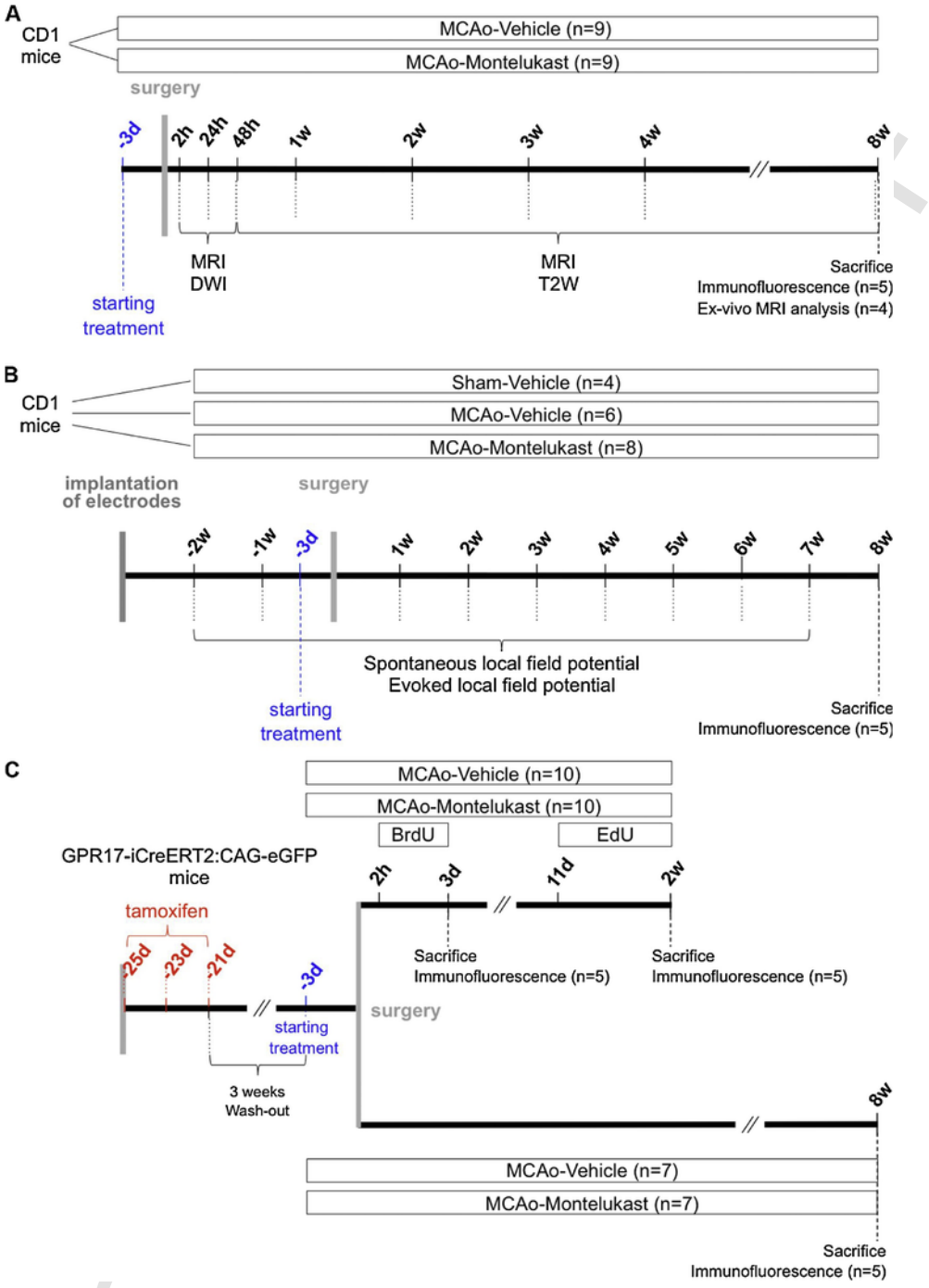

Fig. 1. Outline of the experimental design. **(A)** Time-table of *in-vivo* MRI experiments, immunofluorescence and *ex-vivo* MRI analyses. **(B)** Time-table of electrophysiological recording sessions. **(C)** Time-table of experiment on GPR17-iCreERT2:CAG-eGFP report mice.

Protocol 3 (Fig. 1C). In order to get insight on the effects of montelukast on proliferation or differentiation of OPCs after brain ischemia, we performed MCAo in the conditional reporter GPR17-iCreERT2:CAG-eGFP mouse line [22]. Briefly, mice received 10 mg tamoxifen (Sigma-Aldrich, Taufkirchen, Germany), dissolved in 10% ethanol and 90% corn oil, three times by gavage once every second day. After 3 weeks of wash-out from tamoxifen, mice were underwent permanent MCAo and treated with vehicle (n = 19) or montelukast (n = 18) following the same dosing schedule described above. Two MCAo-Vehicle mice and one MCAo-Montelukast mouse died after surgery.

To study the phenotype of GFP$^+$ proliferating OPCs in the acute phase after ischemic injury, mice (n = 10 for each experimental group) were given four doses of BrdU (Sigma-Aldrich, Taufkirchen, Germany, 50 mg/kg/day i.p.) starting from 2 h up to 3 days after MCAo (Fig. 1C). For immunofluorescence analyses, a group of mice were then sacrificed at 72 h (n = 5 for each experimental group), whereas to also investigate the phenotype of GFP$^+$ proliferating OPCs in the sub-acute phase we labelled cells by administering a second thymidine analog (5-ethynyl-20-deoxyuridine; EdU; Baseclick GmbH, Neuried, Germany) starting from day 11 after MCAo. In particular, mice (n = 5 for each

experimental group) were injected daily with EdU (50 mg/kg/day, i.p.) and sacrificed 4 h after the last injection at 2 weeks after MCAo.

To better characterize the phenotypic changes of the GFP^+-OPCs pool in the chronic phase after ischemic injury, a group of MCAo-Vehicle (n = 7) and MCAo-Montelukast (n = 7) were sacrificed 8 weeks after MCAo.

2.2. In-vivo MRI experiments and data processing

Magnetic resonance imaging (MRI) measurements were performed on a 4.7 T vertical bore MR system (AMX3 Bruker, Ettlingen, Germany). Prior to the experiments, the mice were anesthetized with 2% isofluorane (Merial, Lyon, France) in 70% N_2 and 30% O_2, fixed on a MR-compatible stereotactic holder and placed into a 3.8 cm diameter birdcage coil. Respiration rate was monitored during MRI measurements and body temperature was maintained at 37.0 °C.

Vehicle (n = 9) and MTK (n = 9) treated mice underwent MRI investigations at 2, 24 and 48 h after MCAo for diffusion weighted imaging (DWI) and at 48 h and 1, 2, 3, 4 and 8 weeks after MCAo for T2-weighted (T2W) image.

In details, three different DWIs were acquired using 3 orthogonal diffusion gradient directions; the reference images were identical but without diffusion gradients. Acquisition parameters were: repetition time (TR) = 1500 ms, effective echo time (TE) = 41.2 ms, number of averages (NA) = 4, matrix resolution = 128 × 80, slice thickness = 0.8 mm, interslice distance = 0.8 mm and number of slices = 10. The ischemic volume determination and progression of the ischemic damage over time were performed as previously described [23]. The T2W images were obtained by a fast spin echo sequence with TR = 3000 ms, TE = 80 ms, NA = 8, matrix resolution = 128 × 80, slice thickness = 0.8 mm, interslice distance = 0.8 mm and number of slices = 10. Cerebral atrophy (expressed as percentage) was calculated using the following formula: 100*(L − R)/L, where L (left) is the surface of the contralateral hemisphere and R (right) the surface of the ipsilateral hemisphere.

2.3. Electrophysiological recording and stimulating sessions

For this study, mice were kept in individual cages until the end of the experiments. Animals were anesthetized with 0.8–3% halothane delivered from a calibrated Fluotec 5 vaporizer (Fluotec-Ohmeda) at a flow rate of 1–2 L/min oxygen. As illustrated in Fig. 4A, following stereotaxic coordinates collected from the Paxinos and Franklin atlas, mice were implanted with two recording electrodes (Rec.) in the vibrissal area of the right motor (M1) cortex (1 and 2 mm anterior to bregma, 1.5 and 1.7 mm lateral, and 1 mm depth from brain surface) and with a bipolar stimulating electrode (St.) in the ipsilateral somatosensory barrel (S1) cortex (1 mm posterior to bregma, 2.7 mm lateral, 1 mm depth from brain surface). Electrodes were made from 50 μm, Teflon-coated tungsten wire (Advent Research Materials Ltd, Eynsham, UK). The final location of the recording electrodes was determined using as a guide the field potential depth profile evoked by paired (40 ms of interval) pulses presented to the somatosensory cortex. A bare silver wire (0.1 mm) was affixed to the skull as ground. The four wires were connected to a 4-pin socket and the latter was fixed to the skull with the help of two small screws and dental cement. Further details of this chronic preparation have been reported previously [25].

Recordings were carried out using Grass P511 differential amplifiers with a bandwidth of 0.1 Hz–10 kHz (Grass-Telefactor, West Warwick, USA) using a high-impedance probe (2 × 1012 Ω, 10 pF). Brain stimulation was carried out with the help of a CS-220 stimulator across am ISU-220 isolation unit (Cibertec, Madrid, Spain). Stimulus consisted of single positive-negative (50 μs) pulses applied at intensities >1.0 mA. One week after the implantation of electrodes, animals were randomized in 3 groups: MCAo-Montelukast (n = 8), MCAo-Vehicle (n = 7) and Sham-Vehicle (n = 4) mice and placed in a home-made box (15 × 15 × 10 cm) for baseline electrophysiological recordings. Recording sessions took place one time/week for 9 weeks. Three weeks after implantation of electrodes, mice were subjected to MCAo and sham operation and treated with montelukast or vehicle as described in the *Animal and experimental protocols* section (Fig. 1B).

Recording sessions were organized as follows. In a first step, spontaneous local field potentials were recorded for 5 min with the animal moving freely in the recording box. Afterwards, the animal was presented with a series of 10 electrical stimuli applied to the somatosensory cortex with a minimum interval of 30 s. Spontaneous and evoked local field potentials and 1-volt rectangular pulses corresponding to brain stimulations were stored digitally on a computer through an analog/digital converter (CED 1401 Plus). Spontaneous local field potentials were analyzed off-line with the help of the MatLab 7.4.0 software (MathWorks, Natick, MA, USA). The power spectrum of the cortical LFP activity was computed using the fast Fourier transform with a Hanning window, expressed as relative power and averaged across each recording session. Evoked field potentials were represented and analyzed with the help of the Spike 2 (CED, Milton, UK) program. Five successive field potentials were averaged, and the mean value of the amplitude (in mV) was determined.

2.4. Tissue processing and immunofluorescence analysis

Appropriate tissue processing protocols were applied for immunofluorescence analyses as following:

(i) mice enrolled for *in-vivo* MRI experiment (n = 5 for each group) were sacrificed by transcardiac perfusion using 0.01 M phosphate-buffered saline, pH 7.4 (PBS). Brains were immediately removed and post-fixed with carnoy for 24 h at 4 °C and then embedded in paraffin. Coronal sections of 8 μm were incubated with the primary antibodies rabbit anti-GSTpi (1:500, MBL International, Woburn, MA, USA).

(ii) mice enrolled for electrophysiological experiment (n = 5 for MCAo-Vehicle and MCAo-Montelukast) were sacrificed by transcardiac perfusion using 0.01 M PBS for 10 min and then 4% phosphate-buffered formalin for 10 min. Brains were removed, post-fixed 3 h in 4% phosphate-buffered formalin and cryoprotected in 30% sucrose solution at 4 °C until precipitation. Coronal cryosections of 20 μm were incubated with the primary antibody rat anti-MBP (1:200, Millipore, Billerica, MA, USA).

(iii) GPR17-iCreERT2:CAG-eGFP report mice were sacrificed by transcardiac perfusion using 0.01 M PBS for 10 min and then 4% phosphate-buffered formalin for 25 min. Brains were removed, post-fixed 1 h in 10% phosphate-buffered formalin and cryoprotected in 30% sucrose solution at 4 °C until precipitation.

Double-immunofluorescence were performed on coronal cryosections of 20 μm using chicken anti-GFP (1:1400; Aves Labs, Inc., Tigard, OR, USA) coupled with rabbit anti-cleaved caspase-3 (1:100; Cell Signaling Technology, Danvers, MA, USA), rat anti-BrdU (1:150; Abcam, Cambridge, UK), rabbit anti-GSTpi (1:500; MBL, Woburn, MA, USA), rabbit anti-NG2 (1:2000; Millipore, Temecula, USA) or EdU (Baseclick GmbH, Neuried, Germany, following the manufacturer's instructions). Whereas rabbit anti-Iba1 (1;30,000; Wako Pure Chemical GmbH, Neuss, Germany) were coupled with rabbit anti-Ym1 (1600; StemCell Technologies, Vancouver, Canada) or rat-anti CD16/32 (1:100; BD Pharmigen, San Jose, CA, USA).

For double GFP/BrdU labelling, staining of BrdU was performed first, incubating sections with HCl 2N for 45 min at room temperature.

The signal detection for rabbit anti-NG2 and rabbit anti-Iba1 was performed using High Sensitivity Tyramide Signal Amplification kit (Perkin-Elmer, Monza, Italy; tyramide labelled with tetramethyl-rhodamine for NG2 and tyramide-biotin plus streptavidin-488 for Iba1) following the manufacturer's instructions. For all the other antigens, the signal detection was performed using fluorescent appropriate secondary antibodies coupled to Alexa Fluor 488, Alexa Fluor 555 (both 1:500; Invitrogen, Carlsbad, CA, USA).

Nuclei were labelled with Hoechst 33342 (5 μg/μl, Invitrogen, Carlsbad, CA, USA). Finally, sections were rinsed with PBS and embedded with mounting medium Fluorsave® (Calbiochem, San Diego, CA, USA).

All the immunofluorescence experiments were performed on three coronal brain sections (distant at least 500 μm interval) at a level located within the proximal territory supplied by the MCA from +0.8 to −1.2 mm from bregma for each brain [26].

2.5. Quantitative analysis of the histological and immunofluorescence experiments

After identifying the boundaries of the ischemic lesion we selected specific fields (281.25 μm × 281.25 μm for GFP, 636.40 μm × 636.40 μm for MBP and 325 μm × 435 μm for GSTpi analysis) and acquired images using a confocal microscope (merge of 8-μm z-stack at 2-μm intervals; Nikon A1R, Nikon, Tokyo, Japan) or a fluorescence microscope (200 M; Zeiss, Oberkochen, Germany).

All quantitative analyses were performed using Photoshop CS6 (Adobe System, California, USA) or Fiji, an image-processing package of the open source software ImageJ, by an investigator blinded to the experimental groups.

In detail:

The expression of MBP was evaluated in the regions of cortex, corpus callosum and striatum surrounding the ischemic core (0–636.40 μm from the border of ischemic damage) and expressed as percentage of positive area.

The amount of GSTpi$^+$ cells (cells/μm^2) was expressed as ratio of the number in ipsilateral to contralateral side in order to normalize the data of each different slice. In the ipsilateral side, the measurements were performed for striatum and cortex through the whole peri-infarct zone (0–435 μm from the border of ischemic damage), whereas, for corpus callosum we selected the region close to the ischemic core. The contralateral homologous areas were used as reference since myelinating oligodendrocytes vary with anatomic regions [27].

The number of GFP positive cells was counted in the regions of cortex, corpus callosum and striatum surrounding the ischemic core (0–843.75 μm from the border of ischemic damage). The double-positive GFP/BrdU, GFP/EdU was expressed as the number of positive cells/mm^2, whereas the number of, double-positive GFP/NG2 and GFP/GSTpi cells was calculated and expressed as percentage of GFP positive cells.

The number of double-positive Iba1/YM1 and Iba1/CD16/32 was counted in the proximal (0–281.25 μm from the border of ischemic damage) and in the distal (562.5–843.75 μm from the border of ischemic damage) regions from the ischemic area.

2.6. Ex-vivo MRI analysis and data processing

A group of mice enrolled for *in-vivo* MRI experiment (n = 4 for each group) were anesthetized with ketamine (100 mg/kg) and xylazine (20 mg/kg) at 8 weeks after MCAo and perfused transcardially with 0.01 M PBS containing 10% (w/v) formalin. The intact skulls were excised, soaked in 10% formalin and stored at 4 °C for 24 h. After post-fixation, intact skulls were rinsed in 0.01 M PBS and placed in a custom built plastic tube filled with Fomblin® Y oil (Sigma-Aldrich, Taufkirchen, Germany) – a perfluoropolyether polymer – to reduce MR artefacts and cotton wool to minimize mechanical vibrations. Fixed specimens were acquired with a 3D spin-echo diffusion tensor imaging (DTI) sequence, using the following parameters: TE = 41.74 ms, TR = 1 s, NA = 2, one b_0 image and 19 non-collinear diffusion directions at b = 1800 s/mm^2, data matrix = 104 × 56 × 64 pixels, FOV = 2.6 × 1.4 × 1.6 cm^3 (250 μm^3 isotropic resolution) and acquisition time of approximately 38 h per brain. Morphological images were acquired using a 3D spin-echo scan (TE = 15 ms, TR = 2 s) with same geometry as DTI.

For DTI acquisition scheme, the diffusion gradients orientations were determined by an electrostatic repulsion algorithm, uniformly arranging gradient vectors in space. Such an *ex-vivo* approach allows to increase signal to noise ratio and spatial resolution compared to DTI *in-vivo* analysis [28].

Fractional anisotropy (FA), mean diffusivity (MD), axial diffusivity (λ∥) and radial diffusivity (λ⊥) maps were created from DTI dataset using DSI Studio software [29] and subsequently relative parallel and perpendicular diffusion parameters (D_{par} and D_{per}) were calculated. Previous studies have shown that although fixation reduces the magnitude of water diffusion coefficients (MD, λ∥ and λ⊥) in the brain, it does not alter diffusion anisotropy and relative diffusion parameters [30,31]. FA, D_{par} and D_{per} were calculated in three ribbon-like individual regions of interest (ROIs), including cortex, corpus callosum and striatum. These ROIs were drawn manually surrounding the edge of the lesion for each mouse in three slices of 3D spin-echo scan images taken at level located between +0.8 to -2.2 mm from bregma. These coronal sections were within the proximal territory supplied by the MCA [32] and included the middle enlarged caudoputamen. As control, specular contralateral ROIs were manually traced.

In the same brains, the number of fibers passing through selected ROI in cortex, corpus callosum and striatum, in both hemispheres, was evaluated. For tractography, we used DSI Studio software [29]. Fiber tracts were generated using the following DTI tractography parameters: FA threshold of 0.1 and a turn angle of 55°.

2.7. Statistical analysis

Mice were randomly assigned groups throughout. Data acquisition and analyses were conducted in a blinded manner. Data are reported as mean ± standard deviation (SD). Statistical significance was set at $P < 0.05$.

The multiple comparisons for *in-vivo* and *ex-vivo* diffusion MRI analysis were performed by two-way ANOVA followed by Bonferroni *post-hoc* tests. Statistical analysis of electrophysiological data was performed by one-way ANOVA for repeated measures, with the Friedman repeated measures ANOVA on ranks and/or a contrast analysis (Shaphiro–Wilk test) when necessary.

Fiber tracking, 2 h lesion volume and immunofluorescence data were analyzed with Student's *t*-test.

3. Results

3.1. Montelukast reduces ischemic damage in the acute phase after MCAo

The localization, extension and longitudinal evolution of brain lesion following permanent MCAo were evaluated by diffusion weighted imaging (DWI) MRI analysis performed 2, 24 and 48 h after MCAo in vehicle- (n = 9) and MTK-treated mice (n = 9) (Fig. 2).

At 2 h, montelukast treatment did not affect the volume of the cortical ischemic lesion (31.6 ± 4.8 mm^3) compared to vehicle (30.2 ± 3.9 mm^3).

To reduce intra-subject variability, lesion evolution at 24 and 48 h was evaluated as % variation in infarct volume for each individual ani-

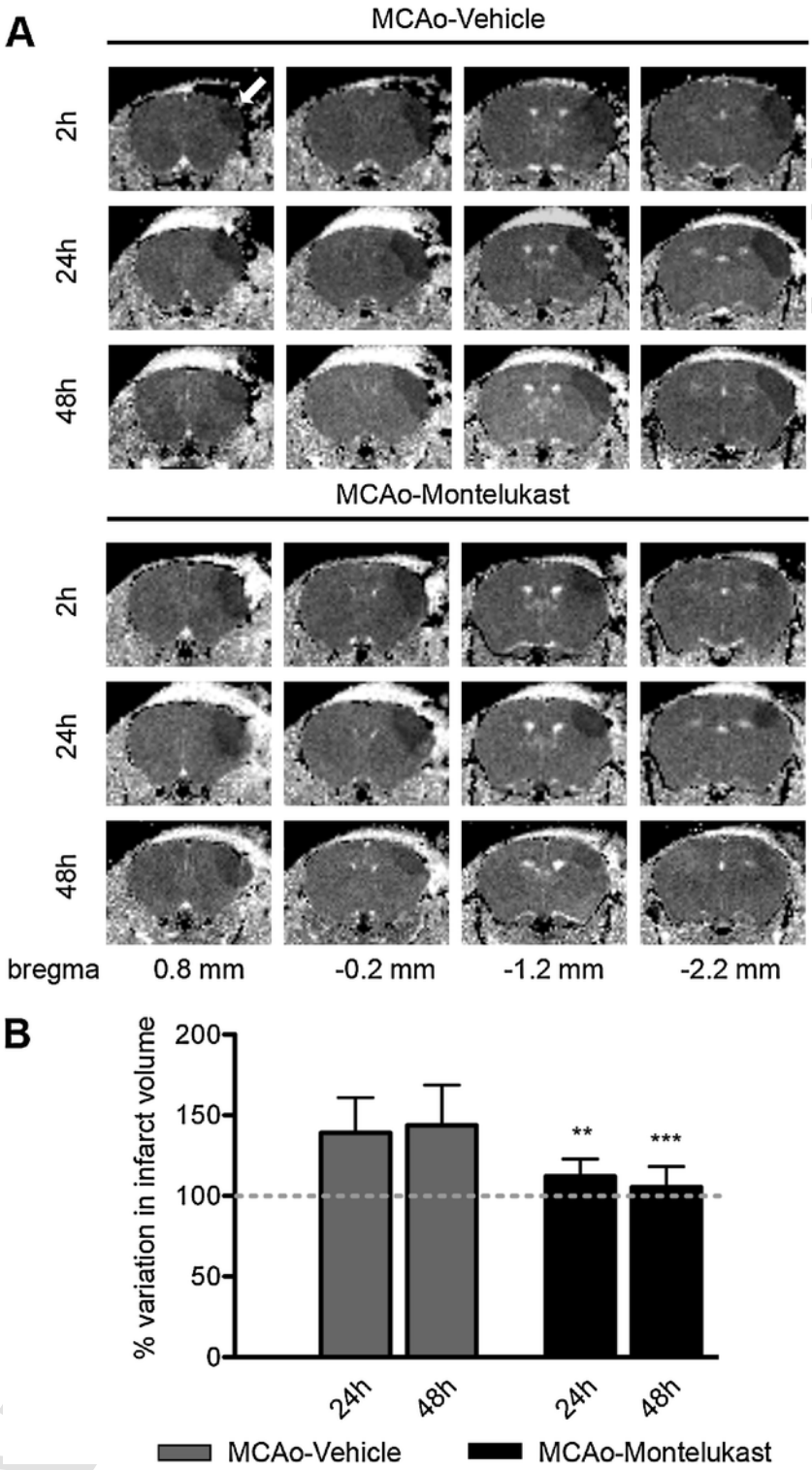

Fig. 2. Infarct volume at acute phases after MCAo. **(A)** DWI-MRI brain coronal sections of a representative mouse treated with vehicle or montelukast taken at four different anatomic levels (+0.80, −0.20, −1.20 and −2.20 mm from bregma) 2, 24, and 48 h after MCAo. The ischemic lesion is detectable as a hypointense area (arrow). **(B)** Bar graph shows the quantitative analysis of the brain damage volume determined by DWI measurements and expressed as percent change relative to the 2 h value set to 100%. Data are shown as mean ± SD (n = 9 mice/each group). Two-way ANOVA analysis followed by Bonferroni *post-hoc* test, ** $P < 0.01$ and *** $P < 0.001$ *versus* MCAo-Vehicle at the corresponding time points.

mal compared to the 2 h value set to 100%. Two-way ANOVA analysis revealed a significant effect of treatment ($P < 0.001$), but not of time and interaction.

In MCAo-Vehicle mice, the volume of brain lesion significantly increased up to 139 ± 22% and to 144 ± 25% at 24 and 48 h, respectively. In contrast, animals receiving MTK showed a smaller increase in brain damage up to 112 ± 11% and 105 ± 13% ($P < 0.01$ and $P < 0.001$ *vs* MCAo-Vehicle by Bonferroni *post-hoc* analysis at 24 and 48 h, respectively (Fig. 2B).

3.2. Montelukast reduces brain damage during the chronic phase after MCAo

Longitudinal T2-weighted (T2W) MRI analysis, revealed the presence of a hyper-intense signal corresponding to ischemia-induced vasogenic edema up to the first week following MCAo. This hyper-intense signal disappeared in the following weeks indicating a resolution of the edema (Fig. 3A).

Further evaluation of brain hemisphere from T2W-images revealed that the ipsilateral side of ischemic mice developed atrophy (Fig. 3A). Two-way ANOVA analysis on data expressed as percentage of atrophy revealed significant effects of time ($P < 0.0001$), treatment ($P < 0.05$), and interaction between these variables ($P < 0.05$).

Specifically, the size of atrophy significantly developed compared to one week after ischemia both in MCAo-Vehicle ($P < 0.001$ by Bonferroni *post-hoc* analysis, for all time points) and MCAo-montelukast ($P < 0.001$ by Bonferroni *post-hoc* analysis, for all time points) groups (Fig. 3B). However, the extent of atrophy was significantly reduced by MTK treatment at 4th and 8th week ($P < 0.05$ *vs* MCAo-Vehicle at the same time points by Bonferroni *post-hoc* analysis; Fig. 3B). No changes in the value of contralateral hemisphere volume were detected (Fig. 1S).

3.3. Montelukast induces faster recovery in local field potential

To gain information on the state of fiber connectivity after MTK treatment, the field potentials evoked in the vibrissal motor cortex area by single pulse stimulation of the ipsilateral barrel area of the somatosensory cortex were measured weekly starting from 2 weeks before MCAo and up to 7 weeks after MCAo (Figs. 1B and 4A). MCAo induced a significant decrease ($P < 0.01$ for weeks 1 and 2 *vs* baseline for both MCAo-Vehicle and MCAo-Montelukast groups) in the amplitude of field potentials that was not recovered in MCAo-Vehicle mice ($P < 0.05$ for week 7 *vs* baseline). Instead, in MCAo-Montelukast mice, this value returned to baseline by the 5th–7th week after stroke (Fig. 4C). In Sham-Vehicle group, no change in the amplitude of field potentials was observed over the experimental period.

As illustrated in Fig. 4D, spontaneous local field potentials recorded before MCAo in the three experimental groups presented a dominant peak in the low theta band (4–6 Hz), characteristic of mice motor and prefrontal cortices [33]. One week after MCAo, mice presented a significant decrease in the amplitude of this dominant theta rhythm, as well as in frequencies >6 Hz ($P < 0.001$ *vs* baseline for both MCAo-Vehicle and MCAo-Montelukast). In MCAo-Vehicle mice there were no signs of recovery up to the final recording sessions (week 6, $P < 0.001$ *vs* baseline), while in MCAo-Montelukast group, local field potentials were recovered at week 6 after MCAo.

3.4. Effect of montelukast on ex-vivo diffusivity parameters and fiber tracking

To evaluate the effects of MTK on brain fibers reorganization, we measured fractional anisotropy (FA) and relative axial (D_{par}) and radial (D_{per}) diffusivity by *ex-vivo* diffusion MRI analysis of brains collected from mice treated with either vehicle or MTK for 8 weeks (Figs. 1A and 5A).

Two-way ANOVA analysis shows that neither ischemia nor MTK treatment induced any significant changes in FA, D_{par} and D_{per} in both corpus callosum and striatum (Fig. 2S). Conversely, ischemia induced a significant increase of FA ($P < 0.001$) and D_{par} ($P < 0.001$) and a significant decrease of D_{per} ($P < 0.001$) in cortex, suggesting fibers reorganization (Fig. 5B). Furthermore, two-way ANOVA analysis revealed an interaction between treatment and hemisphere ($P < 0.05$ for D_{par} and D_{per}) and, in ipsilateral cortex, a significant higher value of D_{par} in

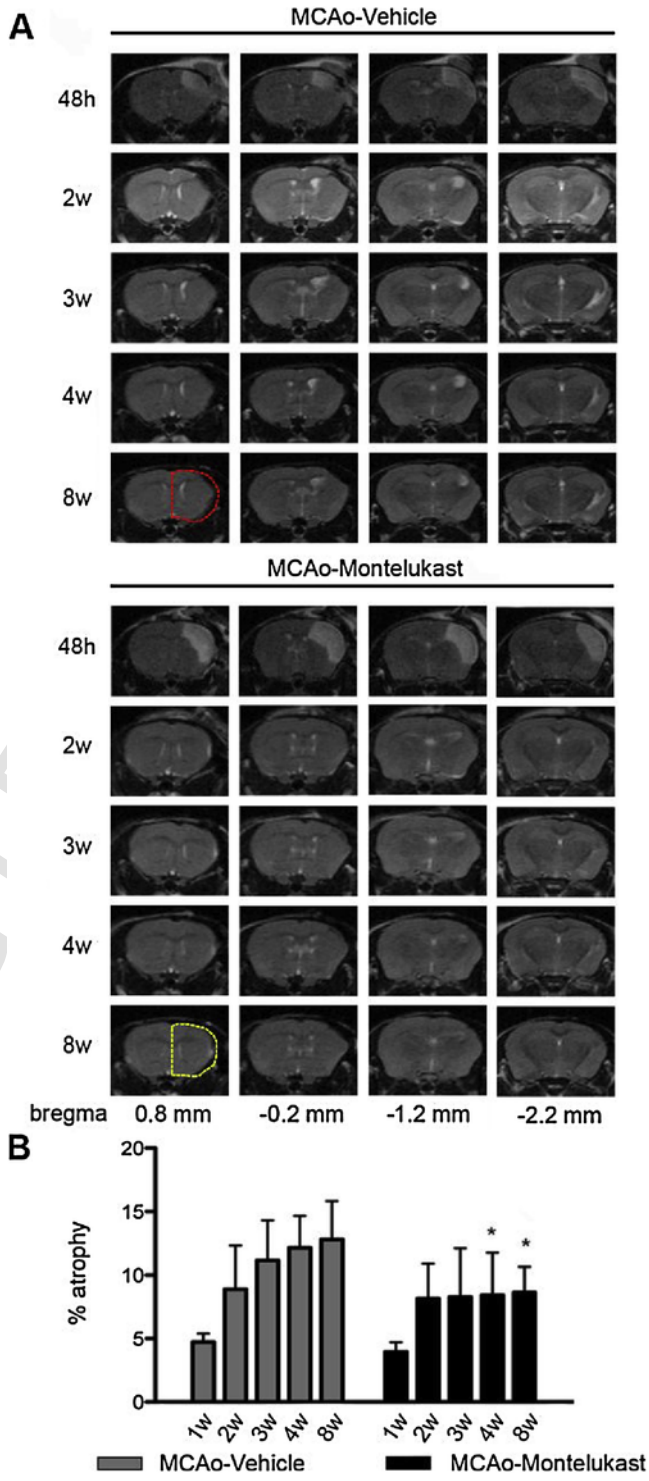

Fig. 3. Brain atrophy size measurements at late phases after MCAo. **(A)** T2W-MRI brain coronal sections of a representative mouse treated with vehicle or montelukast (+0.80, −0.20, −1.20 and −2.20 mm from bregma) at different time points after MCAo. Red (for Vehicle) and yellow (for MTK) dashed lines indicate the manual drawings of the surface of contralateral hemisphere layered on the ipsilateral one. **(B)** Bar graph shows the quantitative analysis of the volume of the brain expressed as relative change of the surface of the contralateral and ipsilateral hemisphere using the formula: 100*(L–R)/L (L = left, contralateral hemisphere; R = right, ipsilateral hemisphere). Data are shown as mean ± SD (n = 9 mice/each group). Two-way ANOVA analysis followed by Bonferroni *post-hoc* test, * $P < 0.05$ *versus* MCAo-Vehicle at the corresponding time point. (For interpretation of the references to colour in this figure legend, the reader is referred to the web version of this article.)

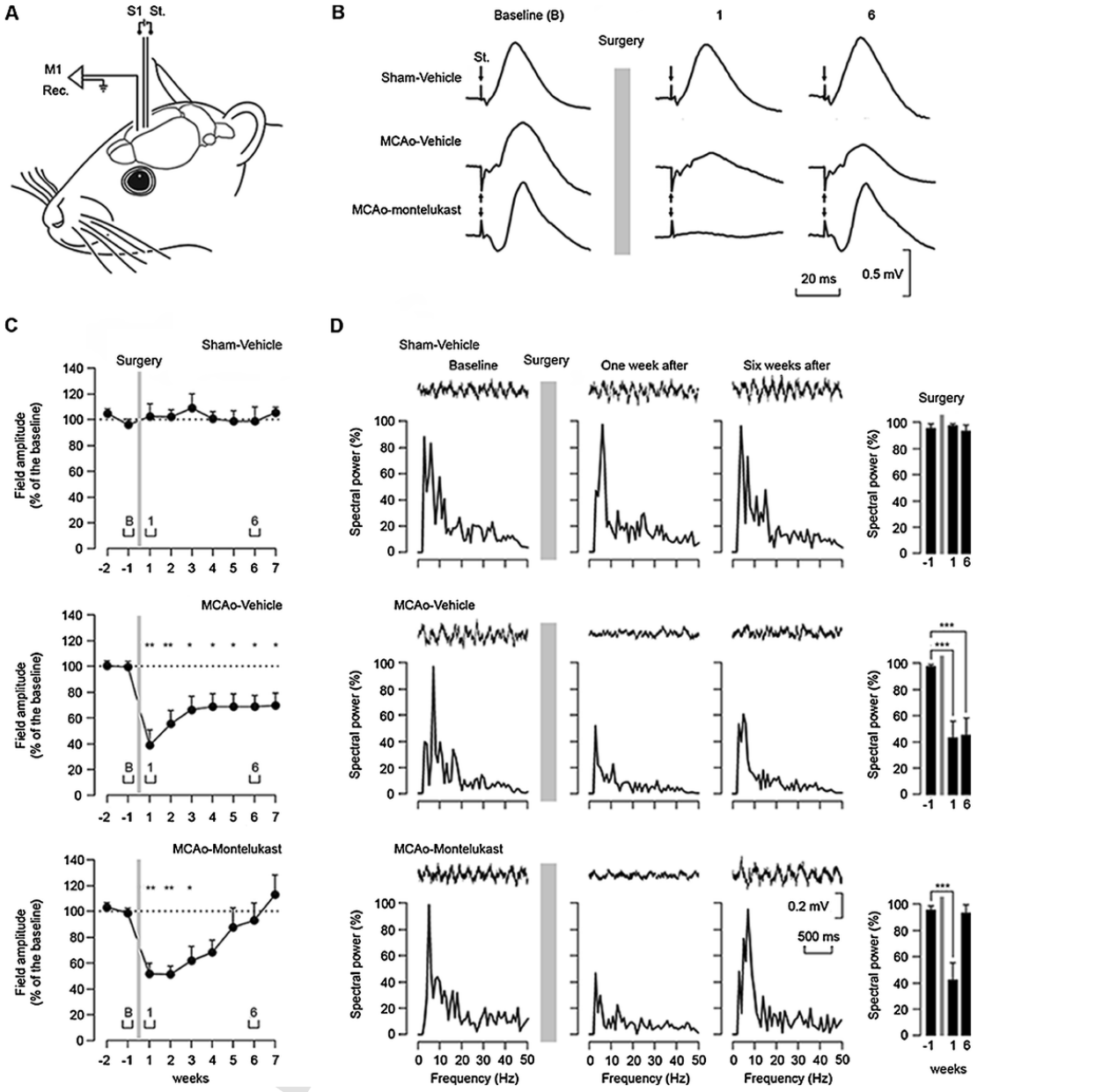

Fig. 4. Effect of montelukast on the evoked and spontaneous local field potentials. **(A)** Animals were chronically implanted with two recording (Rec.) electrodes in the right vibrissal motor cortex (M1) and with bipolar stimulating (St.) electrodes in the ipsilateral somatosensory barrel (S1) cortex. **(B)** Representative examples of field potentials evoked in the M1 area by single pulse stimulation of S1 in the three groups of experimental animals recorded before (Baseline, B) and after surgery (week 1, 6). Calibration bars are shown at the bottom right of the panel. **(C)** The graphs show the evoked field potential amplitudes across recording sessions before surgery (week −2 and −1) and after surgery (from week 1 to week 7). Data are shown as mean ± SD (Sham-Vehicle n = 4 mice; MCAo-Vehicle n = 6 mice; MCAo-montelukast n = 8 mice). One-way ANOVA for repeated measures, *P < 0.05; **P < 0.01 *versus* Baseline. **(D)** Representative examples of spectral powers of spontaneous local field potentials recorded from alert behaving animals before (Baseline) and one and six weeks after surgery. At the top of each spectrum is illustrated a representative example of the field potential recorded in the vibrissal motor cortex. At the right are illustrated the quantitative analysis of averaged power spectra collected from the three experimental groups. Data are shown as mean ± SD (Sham-Vehicle n = 4 mice; MCAo-Vehicle n = 6 mice; MCAo-montelukast n = 8 mice). One-way ANOVA for repeated measures, ***P < 0.001 *versus* baseline (week -1).

MCAo-Montelukast mice compared to the MCAo-Vehicle group (P < 0.05 by Bonferroni *post-hoc* analysis) (Fig. 5B). These data suggest that ischemia-induced brain fibers re-organization is enhanced by MTK treatment.

This drug-mediated effect was further strengthened by fiber tracking evaluation performed on the data obtained by *ex-vivo* diffusion MRI analysis (Fig. 5C). The amount of fibers, expressed as ratio of ipsilateral to contralateral side, was significantly increased in dorsal cortex of MCAo-Montelukast mice (P < 0.05 *vs* MCAo-Vehicle by Bonferroni *post-hoc* analysis) (Fig. 5D). No effect of MTK treatment was observed in the corpus callosum (cc) and striatum. No changes in the number of fibers were detected between MCAo-Vehicle and MCAo-Montelukast groups in the contralateral side (Fig. 3S).

3.5. Effect of montelukast on mature oligodendrocytes

Next, we tested whether the effect of montelukast on electrophysiological connectivity and on diffusivity/fiber tracking is associated with myelin and oligodendrocyte protection. Thus, immunofluorescence staining for MBP (a marker of myelin integrity) and GSTpi (a typical marker of mature myelinating cells) were performed on brain sections collected at 8 weeks from MCAo.

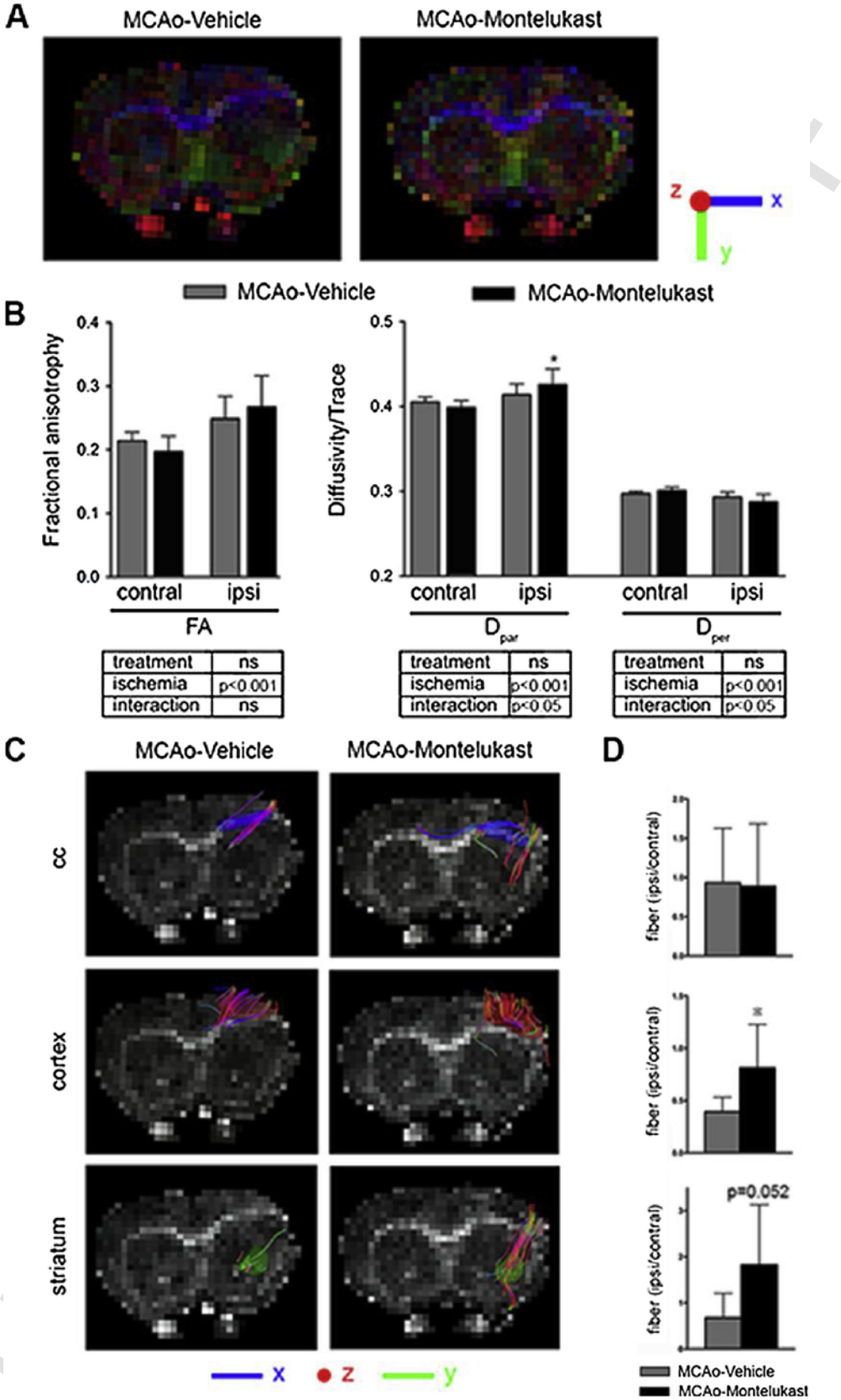

Fig. 5. Effect of montelukast on brain fiber reorganization after MCAo. **(A)** Direction-encoded FA color maps of a representative coronal brain slice at 0.60 mm from bregma of vehicle- or montelukast -treated mouse (red = anterior–posterior direction, blue = left–right, green = superior–inferior). **(B)** Bar graphs show the values of FA and of D_{par} and D_{per}, the axial and radial diffusivity normalized on Trace, respectively, measured in the ipsilateral and contralateral cortex. Data are expressed as mean ± SD (n = 4/each group). Two-way ANOVA analy-

sis followed by Bonferroni *post-hoc* test, * $P < 0.05$ *versus* MCAo-Vehicle ipsilateral. The effect of treatment, ischemia and interaction is reported in the tables below each graph. **(C)** Representative images of three-dimensional fiber tracking in selected ipsilateral ROI (colored area) of corpus callosum (cc), dorsal cortex and striatum in MCAo-Vehicle and MCAo-montelukast mice. The directions of fiber tracks were color-coded as reported at the bottom. **(D)** Bar graphs show the quantification of the number of fibers in ipsilateral normalized to contralateral sides at 8 weeks after MCAo. Data are expressed as mean ± SD (n = 4 mice/each group). Student's *t*-test, * $P < 0.05$ *vs* MCAo-Vehicle. (For interpretation of the references to colour in this figure legend, the reader is referred to the web version of this article.)

Montelukast significantly increased the expression of MBP ($P < 0.05$) compared to vehicle in dorsal cortex (Figs. 6A and 4S), whereas no significant difference of MBP immunoreactivity was observed in either corpus callosum (cc) or striatum.

Similarly, the amount of GSTpi$^+$ cells (expressed as number in ipsilateral/contralateral side) in MCAo-Montelukast group was statistically significant increased compared to MCAo-Vehicle in the dorsal cortex (Fig. 6B), but not in either cc or striatum.

3.6. Effect of montelukast on oligodendrocyte precursor cells (OPCs)

To unveil whether the higher number of mature oligodendrocytes in montelukast-treated mice in the chronic phase after MCAo could be ascribed to an effect of montelukast on oligodendrocyte lineage maturation after MCAo, we analysed the brain section of the inducible reporter GPR17-iCreERT2:CAG-eGFP MCAo mice. These mice are useful for fate-mapping studies, since cells that are OPCs at the moment of tamoxifen administration are permanently labelled by GFP [26] allowing us to trace their destiny throughout animal's life.

Our data confirmed that MCAo dramatically increased the number of GFP$^+$ OPCs in the peri-infarct areas (dorsal cortex, cc and striatum) at 2 weeks (Fig. 5S) [26], and this response was further enhanced by montelukast treatment ($P < 0.05$ in corpus callosum; Fig. 7A).

Then, we sought to determine which mechanism was related to the increased number of GFP$^+$ OPCs, investigating cellular proliferation and apoptosis. We assessed OPC proliferation in the acute (within 3 days) and in the sub-acute (between 11 and 14 days) phases of brain ischemia, evaluating BrdU and EdU cellular incorporation at 2 weeks after MCAo, respectively. Montelukast significantly stimulated OPC proliferation, as reflected by increased numbers of BrdU$^+$/GFP$^+$ cells in corpus callosum ($P < 0.05$; Fig. 7B) and of EdU$^+$/GFP$^+$ cells in dorsal cortex ($P < 0.01$; Fig. 7B), compared to MCAo-Vehicle group. On the other hand, montelukast did not influence apoptotic process of GFP$^+$ OPCs at 3 days after MCAo since no statistical difference was found on the number of GFP$^+$/caspase-3a$^+$ cells between MCAo-Montelukast and MCAo-Vehicle groups (Fig. 6S).

Since oligodendrocyte lineage maturation is fundamental for remyelination and functional recovery after stroke, we assessed whether the recombined GFP$^+$ OPCs cells are able to undergo terminal differentiation at sub-acute (2 weeks) and chronic (8 weeks) phases of brain ischemia. At 2 weeks, we found that montelukast does not influence the fate of OPCs; in fact, the percentage of GFP$^+$ cells expressing NG2 (marker of early OPCs) or GSTpi was not different between MCAo-Montelukast and MCAo-Vehicle groups (Fig. 7C). At 8 weeks, however, the percentage of GFP$^+$/GSTpi$^+$ cells raised significantly in MCAo-Montelukast group compared to MCAo-Vehicle group ($P < 0.05$;

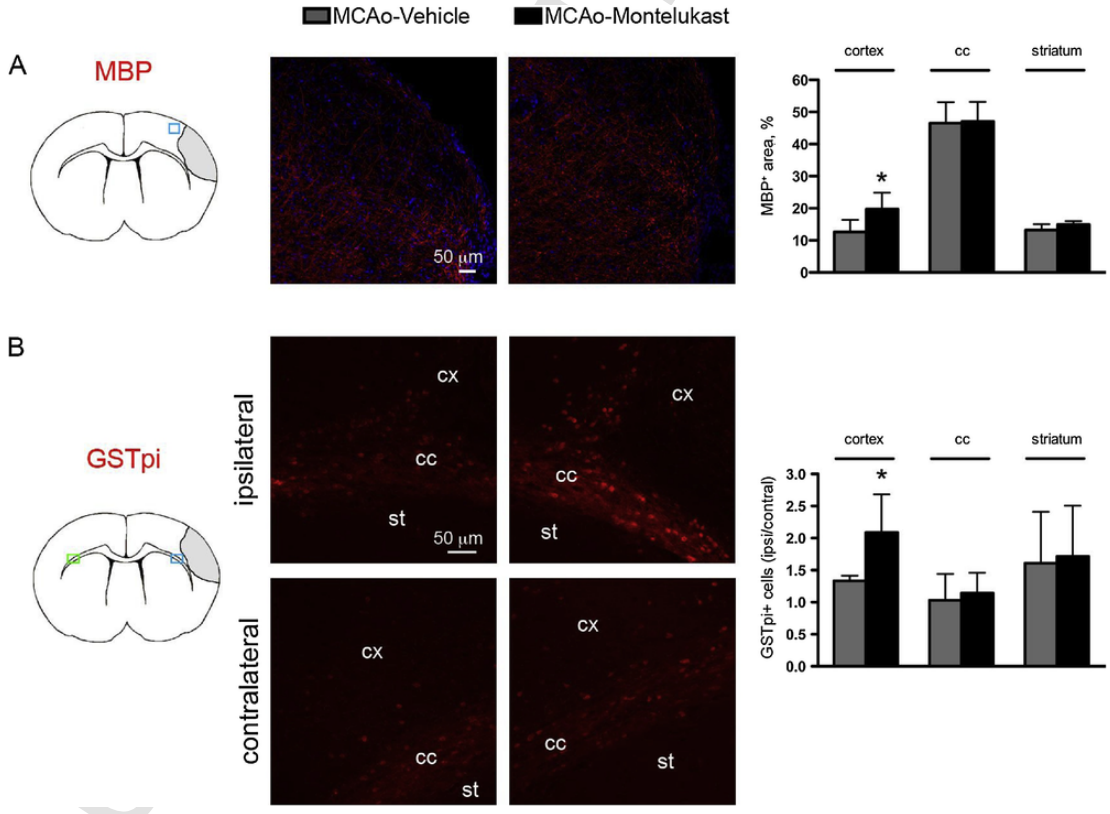

Fig. 6. Effect of montelukast on oligodendrocytes at 8 weeks after MCAo. **(A)** Representative images of immunofluorescence staining for MBP (in red) in a field containing ipsilateral cortex taken as shown in drawing (blue square) of MCAo-Vehicle and MCAo-Montelukast mice. Bar graphs report the quantification of the percentage of positive area in cortex, corpus callosum (cc) and striatum. **(B)** Representative images of immunofluorescence staining for GSTpi (red), in a field containing cortex (cx), corpus callosum (cc) and striatum (st), taken as shown in drawing from ipsilateral (blue rectangle) and contralateral (green rectangle) of MCAo-Vehicle and MCAo-Montelukast mice. Bar graph reports the quantification of the number of GSTpi$^+$ cells in ipsilateral normalized to contralateral regions. Data are expressed as mean ± SD (n = 5/groups). Student's *t*-test * $P < 0.05$ *vs* MCAo-Vehicle. Scale bar: 50 μm. (For interpretation of the references to colour in this figure legend, the reader is referred to the web version of this article.)

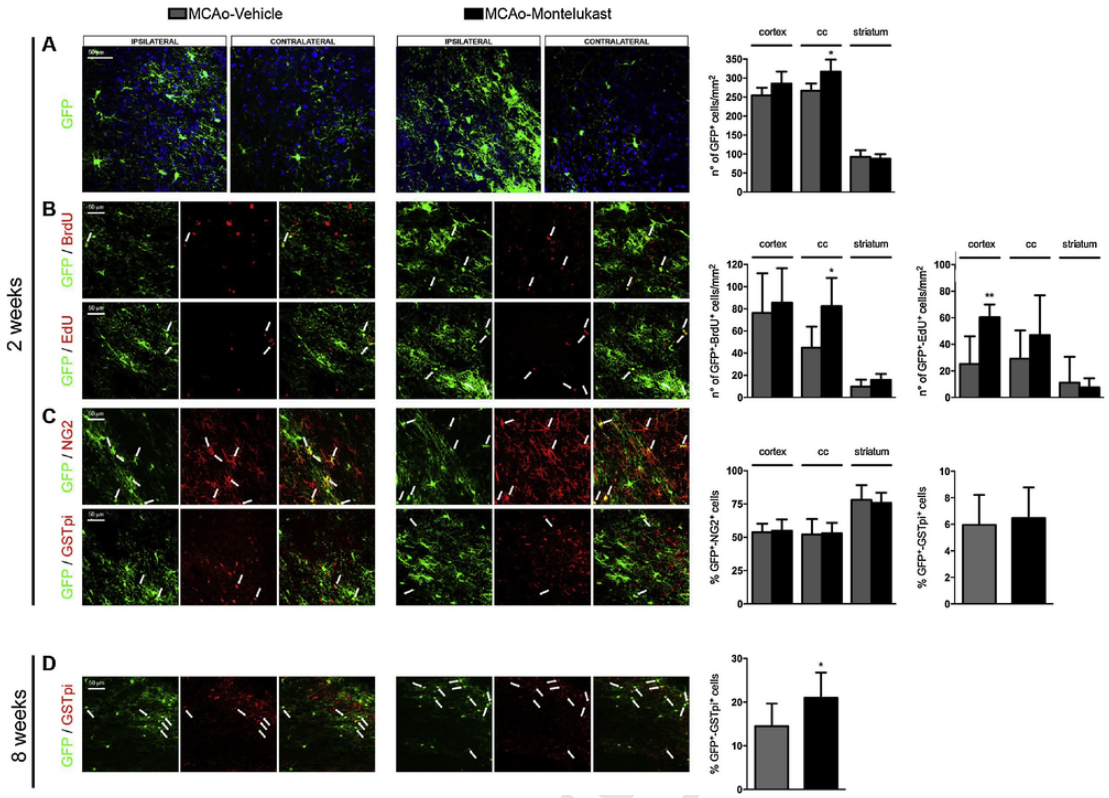

Fig. 7. Effect of montelukast on oligodendrocyte precursor cells (OPCs) after MCAo. Representative images of immunofluorescence in fields containing cortex, corpus callosum (cc) and striatum of MCAo-Vehicle and MCAo-Montelukast mice. Arrows show double-positive cells. **(A)** Staining for GFP (green) in ipsilateral and contralateral side 2 weeks after MCAo. Bar graphs report the quantification of the number of GFP^+ cells in ipsilateral regions (**B**) Double-immunofluorescence staining for BrdU (red) (upper line) or EdU (red) (lower line) and for GFP (green) in ipsilateral regions surrounding the ischemic core 2 weeks after MCAo. Bar graphs report the quantification of the number of double GFP^+- $BrdU^+$ cells and double GFP^+- EdU^+ cells in ipsilateral cortex, cc and striatum. **(C)** Double-immunofluorescence staining for NG2 (red) (upper line) or GSTpi (red) (lower line) and for GFP (green) in ipsilateral regions surrounding the ischemic core 2 weeks after MCAo. Bar graphs report the percentage of GFP^+- $NG2^+$ over GFP^+ cells in ipsilateral cortex, cc and striatum, and the percentage of GFP^+- $GSTpi^+$ cells over GFP^+ cells in the whole peri-infarct zone. (**D**) Double-immunofluorescence staining for GFP (green) and $GSTpi^+$ (red) in ipsilateral regions surrounding the ischemic core 8 weeks after MCAo. Bar graphs report the percentage of GFP^+- $GSTpi^+$ cells over GFP^+ cells in the whole peri-infarct zone. Data are expressed as mean ± SD (n = 5/groups). Student's *t*-test * $P < 0.05$, ** $P < 0.01$ *vs* MCAo-Vehicle. Scale bar: 50 μm. (For interpretation of the references to colour in this figure legend, the reader is referred to the web version of this article.)

Fig. 7D), suggesting that montelukast could increase oligodendrocyte replacement after MCAo.

3.7. Montelukast enhances M2 polarized microglia after ischemia

Recent studies have demonstrated the role of microglia/macrophages in recruitment and differentiation of OPCs, leading remyelination [34]. In particular, has been shown that the M1 phenotype impairs oligodendrocytes regeneration, while M2 phenotype promotes oligodendrogenesis and remyelination [35].

Thus, we investigated whether montelukast is able to regulate microglia/macrophage polarization after stroke evaluating the expression of CD16/32 and YM1 for M1 and M2, respectively [36]. Montelukast treatment significantly increased the numbers of M2 polarized microglia/macrophages, labeled for Iba1 and YM1, in the proximal region at 3 days after MCAo ($P < 0.05$; Fig. 8A). No montelukast-mediated effect was observed on the number of M1 polarized microglia/macrophages, labeled for Iba1 and CD16/32 (Fig. 8B).

4. Discussion

We have previously shown that montelukast reduces the extent of brain damage in the acute phase of ischemic injury [9], as also confirmed by other groups [11,24]. In this study, we focused on the

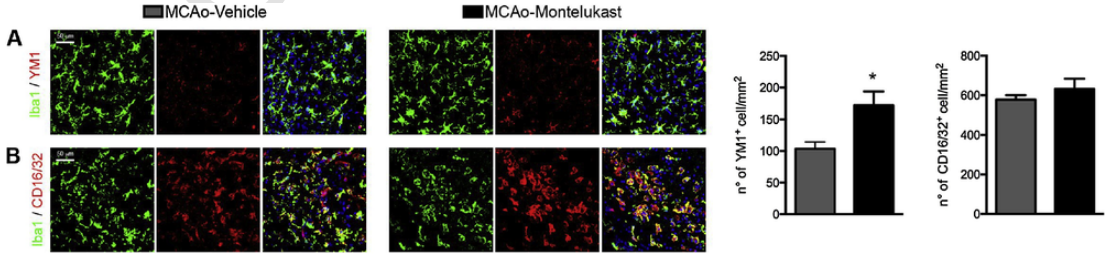

Fig. 8. Effect of montelukast on microglia/macrophages polarization 3 days after MCAo. Representative images of immunofluorescence for YM1 (red) **(A)** or CD16/32 (red) **(B)** and for Iba1 (green) in regions surrounding the ischemic core of MCAo-Vehicle and MCAo-Montelukast mice. Bar graphs report the quantification of the number of $YM1^+$ and $CD16/32^+$ cells. Data are expressed as mean ± SD (n = 5/groups). Student's *t*-test * $P < 0.05$ *vs* MCAo-Vehicle. Scale bar: 50 μm. (For interpretation of the references to colour in this figure legend, the reader is referred to the web version of this article.)

long-term protective effect of montelukast on fibers re-organization and electrophysiological transmission in MCAo mice. Furthermore, we investigated the effect of montelukast on oligodendrocytes, the myelin producing cells, a yet unexplored target for neuro-reparative strategies after brain ischemia.

In order to block the effects related to early [6] and chronic CysLTs release after ischemia, montelukast was administered before and after MCAo. The pre-treatment is justified by pharmacokinetic data collected in rodents, indicating that montelukast is able to cross intact blood brain barrier and, even if it has a short half-life, needs hours to accumulate in brain [37]. Moreover, montelukast pre-treatment did not affect the susceptibility to ischemia, since no difference was observed in the size of ischemic lesion at 2 h after MCAo in montelukast- and vehicle-treated mice.

In line with previous results [10], montelukast exerted long-term protection against the severe brain atrophy developing after stroke. However, since drug-induced reductions in ischemic lesion volume do not necessarily imply any improvement in animals' functional outcome, which is instead an essential requisite to prove drug efficacy [38], we showed that montelukast-induced amelioration of brain atrophy was also associated to restoration of cortical field potentials, as evaluated by electrophysiological tests. Specifically, we reported for the first time, that, in living and freely-moving mice, induction of brain ischemia was associated to early and chronic reduction in the amplitude of evoked field potentials, as well as of spontaneous local field potentials. We also showed that both these alterations were restored to control level by chronic montelukast treatment, suggesting that chronic drug administration induces recovery of cell connectivity in the regions surrounding the ischemic lesion. To support this hypothesis, we also implemented the montelukast-induced functional effects with data on structure connectivity, obtained by *ex-vivo* MRI analyses performed to evaluate DTI parameters and fiber tracking. DTI data analyses revealed that, 8 weeks after stroke, there was an increase of FA and D_{par} values and a decrease of D_{per} values in ipsilateral motor cortex, suggesting, in line with previous observations [28], spontaneous fibers re-organization in the region surrounding the ischemic area. Ischemia-induced changes of these parameters were enhanced by montelukast treatment. Although no differences in FA and D_{per} mean values were observed between vehicle and montelukast-treated mice in the ipsilateral cortex, the value of D_{par} was significantly higher in montelukast-treated mice compared to vehicle. This apparent inconsistency between FA and directional diffusivity has been already described in other models of neurodegeneration [39] and could indicate that, in addition to FA, diffusivity parameters should be considered as indices of ischemic-induced axonal and myelin damage at chronic stages [40]. The effect of montelukast on fiber re-organization was also confirmed by DTI-fiber tracking analysis revealing that the drug increased the number of fibers in the ipsilateral cortex compared to vehicle. These data suggested that montelukast is able to either prevent and/or repair fiber disruption, thus contrasting the loss of connectivity occurring in the ischemic cerebral cortex.

Previous DTI studies have demonstrated that, after ischemia, cerebral tissues show a reduction in both myelin content and number of oligodendrocytes [41]. Our DTI and electrophysiology data now provided direct evidence of altered structural and functional connectivity in the regions around ischemic lesions in rodents, indicating that, besides neurons, oligodendrocytes are also highly susceptible to ischemic insults [14] and thus emphasizing the role of oligodendroglial cells and myelination in neural connectivity [17]. Thus, protection or recovery of white matter could promote neurological functions, including sensorimotor functions, by enhancing the electrophysiological transmission of neuronal signals between different brain areas.

In this study we reported that montelukast improves white matter integrity increasing the number of mature oligodendrocytes and possibly reducing myelin loss, as shown by higher expression of MBP in the ipsilateral dorsal cortex of MCAo-Montelukast mice. In the ipsilateral cortex of vehicle-treated mice, we observed a slight increase in the number of mature $GSTpi^+$ oligodendrocytes compared to contralateral regions, likely indicating an attempt to respond to oligodendrocyte injury. Although with some differences, this is in line with previous data reporting hypoperfusion-induced white matter lesions in rats after bilateral common carotid artery ligation [42], suggesting involvement of oligodendrocytes in post-ischemic remodelling of cerebral tissue. Our data, showing that montelukast further amplified this response, significantly increasing the number of $GSTpi^+$ cells in the ipsilateral cortex compared to vehicle, strengthened this hypothesis.

The mechanisms underlying montelukast-mediated white matter recovery could be manifold. Firstly, we observed an increased recruitment of OPCs in peri-ischemic areas that was significantly enhanced by montelukast treatment. In this regard, we demonstrated that montelukast increased the proliferation of OPCs in the acute and sub-acute phase after ischemia. This data is corroborated by a recent study showing that montelukast stimulates proliferation of precursors cells in the hippocampal dentate gyrus of aged rodents and that this effect resulted in cognitive improvement [13]. This observation is further sustained by other pharmacological studies showing that improvement of long-term neurological functions could be enhanced by OPC proliferation [14,43]. However, we can't rule out also a possible effect of montelukast on cellular migration in the increased recruitment of OPCs.

Secondly, we showed for the first time that montelukast, in the chronic phase of stroke, increased the maturation of recruited OPCs. Stroke, itself, leads the proliferation of OPCs [44], but most of them fail to reach maturation, resulting in poor white matter recovery [45]. In our hypothesis, it is unlikely that montelukast drives differentiation acting directly on OPCs. Indeed, in our unpublished data, montelukast was not able to overcome the block of differentiation induced by TNF-α in OPC culture, suggesting a possible involvement of other cells. Substantial evidence shows that microglia/macrophages modulates maturation of oligodendrocyte during CNS remyelination [43,46,47], and it is widely accepted that microglia/macrophages M2 phenotype promotes oligodendrogenesis and OPCs maturation, while the microglia/macrophages M1 phenotype impairs oligodendrocytes regeneration [35,48]. At 3 days after MCAo, our data showed that montelukast increased the number of M2 microglia/macrophages, suggesting that OPC differentiation observed could be an indirect microglia-mediated effect. This aspect is particularly relevant and the molecular and cellular crosstalk mechanisms needs to be further investigated in future studies. Indeed, montelukast is not only an antagonist of CysLTR-1, but also of other targets, such as GPR17 and PDEs [9,49]. These receptors are localized in different CNS cells and their expression or activation changes after stroke [49]. Thus, montelukast may offer improved therapeutic efficacy, targeting different cell types and multiple functions affected by stroke.

In summary, we showed that the already marketed and safe anti-asthmatic drug montelukast improves spontaneous long-term electrophysiological recovery in ischemic mice by preserving brain fibers connectivity and white matter integrity. These beneficial effects can be ascribed to a double action of montelukast on OPCs. Firstly, montelukast increased the pool of OPCs available for full maturation, enhancing their proliferation, and secondly, it promoted likely by an indirect manner oligodendrocyte differentiation.

Together with the previous observed neuroprotective effects of montelukast, such as decrease of oxidative stress, inflammation and release of glutamate [49], our findings, mostly concentrated on glial cells, could comprehensively explain the ability of montelukast to lead long-term recovery after stroke.

However, our *in-vivo* experimental plan does not allow us to define whether the beneficial effects of montelukast treatment could be as-

cribed to an acute or chronic action of the drug. Furthermore, the experimental setting used in the present study does not allow to ascertain whether the enhanced OPCs differentiation is a direct effect of montelukast on these cells or is related to changes in the microglial phenotype. Further studies are needed to evaluate the direct effect of montelukast on microglial polarization and the underlying mechanisms.

In our opinion, these data provide the rationale for montelukast "repurposing" in this and other neurodegenerative diseases, substantially reducing the risk, times and costs associated with the development of new safe and effective drugs. In this respect, the dose chronically administered in this study was the same that was effective in a murine model of asthma [50].

More in general, our data open up new pharmacological opportunities to treat stroke focusing on oligodendrocyte protection and white matter reorganization.

Disclosure

None.

Acknowledgements

This study was partially funded by the ERA-NET "Network of European Funding for Neuroscience Research" (NEURON) project "RENEW IT", and by the Cariplo Foundation (Ref N. 2012-0546 to LS and Ref. N. 2015-0910 to MF and PG). We thank Mr. José M. González-Martín, Ms. María Sánchez-Enciso and Ms. Olga Palomo-Casillas for their held in animal handle and care and in the performance of the electrophysiological and behavioural experiments. We thank Raffaella Iacubino for excellent technical assistance.

Part of this work was carried out in NOLIMITS, an advanced microscopy laboratory established by University of Milan.

Appendix A. Supplementary data

Supplementary material related to this article can be found, in the online version, at doi:https://doi.org/10.1016/j.phrs.2019.02.025.

References

[1] J. Mackay, G. Mensah, K. Greenlund, The Atlas of Heart Disease and Stroke, World Health Organization, Geneva, 2004.
[2] G.H. Danton, W.D. Dietrich, Inflammatory mechanisms after ischemia and stroke, J. Neuropathol. Exp. Neurol. 62 (2) (2003) 127–136.
[3] W.D. Heiss, The ischemic penumbra: how does tissue injury evolve?, Ann. N. Y. Acad. Sci. 1268 (2012) 26–34.
[4] M. Certo, Y. Endo, K. Ohta, S. Sakurada, G. Bagetta, D. Amantea, Activation of RXR/PPARgamma underlies neuroprotection by bexarotene in ischemic stroke, Pharmacol. Res. 102 (2015) 298–307.
[5] N.A. Berger, V.C. Besson, A.H. Boulares, A. Burkle, A. Chiarugi, R.S. Clark, N.J. Curtin, S. Cuzzocrea, T.M. Dawson, V.L. Dawson, G. Hasko, L. Liaudet, F. Moroni, P. Pacher, P. Radermacher, A.L. Salzman, S.H. Snyder, F.G. Soriano, R.P. Strosznajder, B. Sumegi, R.A. Swanson, C. Szabo, Opportunities for the repurposing of PARP inhibitors for the therapy of non-oncological diseases, Br. J. Pharmacol. 175 (2) (2018) 192–222.
[6] P. Ciceri, M. Rabuffetti, A. Monopoli, S. Nicosia, Production of leukotrienes in a model of focal cerebral ischaemia in the rat, Br. J. Pharmacol. 133 (8) (2001) 1323–1329.
[7] T. Baba, K.L. Black, K. Ikezaki, K.N. Chen, D.P. Becker, Intracarotid infusion of leukotriene C4 selectively increases blood-brain barrier permeability after focal ischemia in rats, J. Cereb. Blood Flow. Metab. 11 (4) (1991) 638–643.
[8] C.E. Corser-Jensen, D.J. Goodell, R.K. Freund, P. Serbedzija, R.C. Murphy, S.E. Farias, M.L. Dell'Acqua, L.C. Frey, N. Serkova, K.A. Heidenreich, Blocking leukotriene synthesis attenuates the pathophysiology of traumatic brain injury and associated cognitive deficits, Exp. Neurol. 256 (2014) 7–16.
[9] P. Ciana, M. Fumagalli, M.L. Trincavelli, C. Verderio, P. Rosa, D. Lecca, S. Ferrario, C. Parravicini, V. Capra, P. Gelosa, U. Guerrini, S. Belcredito, M. Cimino, L. Sironi, E. Tremoli, G.E. Rovati, C. Martini, M.P. Abbracchio, The orphan receptor GPR17 identified as a new dual uracil nucleotides/cysteinyl-leukotrienes receptor, EMBO J. 25 (19) (2006) 4615–4627.
[10] R. Zhao, W.Z. Shi, Y.M. Zhang, S.H. Fang, E.Q. Wei, Montelukast, a cysteinyl leukotriene receptor-1 antagonist, attenuates chronic brain injury after focal cerebral ischaemia in mice and rats, J. Pharm. Pharmacol. 63 (4) (2011) 550–557.
[11] M.A. Saad, R.M. Abdelsalam, S.A. Kenawy, A.S. Attia, Montelukast, a cysteinyl leukotriene receptor-1 antagonist protects against hippocampal injury induced by transient global cerebral ischemia and reperfusion in rats, Neurochem. Res. 40 (1) (2015) 139–150.
[12] E. Ingelsson, L. Yin, M. Back, Nationwide cohort study of the leukotriene receptor antagonist montelukast and incident or recurrent cardiovascular disease, J. Allergy Clin. Immun. 129 (3) (2012), 702–707.e2.
[13] J. Marschallinger, I. Schaffner, B. Klein, R. Gelfert, F.J. Rivera, S. Illes, L. Grassner, M. Janssen, P. Rotheneichner, C. Schmuckermair, R. Coras, M. Boccazzi, M. Chishty, F.B. Lagler, M. Renic, H.C. Bauer, N. Singewald, I. Blumcke, U. Bogdahn, S. Couillard-Despres, D.C. Lie, M.P. Abbracchio, L. Aigner, Structural and functional rejuvenation of the aged brain by an approved anti-asthmatic drug, Nat. Commun. 6 (2015) 8466.
[14] L. Zhang, M. Chopp, R.L. Zhang, L. Wang, J. Zhang, Y. Wang, Y. Toh, M. Santra, M. Lu, Z.G. Zhang, Erythropoietin amplifies stroke-induced oligodendrogenesis in the rat, PLoS One 5 (6) (2010) e11016.
[15] D. Leys, E. Englund, T. Del Ser, D. Inzitari, F. Fazekas, N. Bornstein, T. Erkinjuntti, J.V. Bowler, L. Pantoni, L. Parnetti, J. De Reuck, J. Ferro, J. Bogousslavsky, White matter changes in stroke patients. Relationship with stroke subtype and outcome, Eur. Neurol. 42 (2) (1999) 67–75.
[16] X.S. Liu, M. Chopp, H. Kassis, L.F. Jia, A. Hozeska-Solgot, R.L. Zhang, C. Chen, Y.S. Cui, Z.G. Zhang, Valproic acid increases white matter repair and neurogenesis after stroke, Neuroscience 220 (2012) 313–321.
[17] S. Rosenzweig, S.T. Carmichael, The axon-glia unit in white matter stroke: mechanisms of damage and recovery, Brain Res. 1623 (2015) 123–134.
[18] S. Falahati, M. Breu, A.T. Waickman, A.W. Phillips, E.J. Arauz, S. Snyder, M. Porambo, K. Goeral, A.M. Comi, M.A. Wilson, M.V. Johnston, A. Fatemi, Ischemia-induced neuroinflammation is associated with disrupted development of oligodendrocyte progenitors in a model of periventricular leukomalacia, Dev. Neurosci. 35 (2–3) (2013) 182–196.
[19] F. Labombarda, S. Gonzalez, A. Lima, P. Roig, R. Guennoun, M. Schumacher, A.F. De Nicola, Progesterone attenuates astro- and microgliosis and enhances oligodendrocyte differentiation following spinal cord injury, Exp. Neurol. 231 (1) (2011) 135–146.
[20] M. Fumagalli, D. Lecca, G.T. Coppolino, C. Parravicini, M.P. Abbracchio, Pharmacological properties and biological functions of the GPR17 receptor, a potential target for neuro-regenerative medicine, Adv. Exp. Med. Biol. 1051 (2017) 169–192.
[21] M.S. Seyedsadr, B.V. Ineichen, Gpr17, a player in lysolecithin-induced demyelination, oligodendrocyte survival, and differentiation, J. Neurosci. 37 (9) (2017) 2273–2275.
[22] F. Vigano, S. Schneider, M. Cimino, E. Bonfanti, P. Gelosa, L. Sironi, M.P. Abbracchio, L. Dimou, GPR17 expressing NG2-glia: oligodendrocyte progenitors serving as a reserve pool after injury, Glia 64 (2) (2016) 287–299.
[23] L. Sironi, M. Cimino, U. Guerrini, A.M. Calvio, B. Lodetti, M. Asdente, W. Balduini, R. Paoletti, E. Tremoli, Treatment with statins after induction of focal ischemia in rats reduces the extent of brain damage, Arterioscler Thromb. Vasc. Biol. 23 (2) (2003) 322–327.
[24] G.L. Yu, E.Q. Wei, S.H. Zhang, H.M. Xu, L.S. Chu, W.P. Zhang, Q. Zhang, Z. Chen, R.H. Mei, M.H. Zhao, Montelukast, a cysteinyl leukotriene receptor-1 antagonist, dose- and time-dependently protects against focal cerebral ischemia in mice, Pharmacology 73 (1) (2005) 31–40.
[25] J. Troncoso, A. Munera, J.M. Delgado-Garcia, Learning-dependent potentiation in the vibrissal motor cortex is closely related to the acquisition of conditioned whisker responses in behaving mice, Learn. Mem. 14 (1) (2007) 84–93.
[26] E. Bonfanti, P. Gelosa, M. Fumagalli, L. Dimou, F. Vigano, E. Tremoli, M. Cimino, L. Sironi, M.P. Abbracchio, The role of oligodendrocyte precursor cells expressing the GPR17 receptor in brain remodeling after stroke, Cell Death Dis. 8 (6) (2017) e2871.
[27] D.C. Morris, M. Chopp, L. Zhang, M. Lu, Z.G. Zhang, Thymosin beta4 improves functional neurological outcome in a rat model of embolic stroke, Neuroscience 169 (2) (2010) 674–682.
[28] J. Zhang, Diffusion tensor imaging of white matter pathology in the mouse brain, Imaging Med. 2 (6) (2010) 623–632.
[29] F.C. Yeh, T.D. Verstynen, Y. Wang, J.C. Fernandez-Miranda, W.Y. Tseng, Deterministic diffusion fiber tracking improved by quantitative anisotropy, PLoS One 8 (11) (2013) e80713.
[30] S.W. Sun, J.J. Neil, H.F. Liang, Y.Y. He, R.E. Schmidt, C.Y. Hsu, S.K. Song, Formalin fixation alters water diffusion coefficient magnitude but not anisotropy in infarcted brain, Magn. Reson. Med. 53 (6) (2005) 1447–1451.
[31] S.W. Sun, J.J. Neil, S.K. Song, Relative indices of water diffusion anisotropy are equivalent in live and formalin-fixed mouse brains, Magn. Reson. Med. 50 (4) (2003) 743–748.
[32] M. Kuraoka, T. Furuta, T. Matsuwaki, T. Omatsu, Y. Ishii, S. Kyuwa, Y. Yoshikawa, Direct experimental occlusion of the distal middle cerebral artery induces high reproducibility of brain ischemia in mice, Exp. Anim. 58 (1) (2009) 19–29.
[33] N. Karalis, C. Dejean, F. Chaudun, S. Khoder, R.R. Rozeske, H. Wurtz, S. Bagur, K. Benchenane, A. Sirota, J. Courtin, C. Herry, 4-Hz oscillations synchronize prefrontal-amygdala circuits during fear behavior, Nat. Neurosci. 19 (4) (2016) 605–612.
[34] V.E. Miron, Microglia-driven regulation of oligodendrocyte lineage cells, myelination, and remyelination, J. Leukocyte Biol. 101 (5) (2017) 1103–1108.

[35] X. Hu, R.K. Leak, Y. Shi, J. Suenaga, Y. Gao, P. Zheng, J. Chen, Microglial and macrophage polarization-new prospects for brain repair, Nat. Rev. Neurol. 11 (1) (2015) 56–64.
[36] A. Villa, P. Gelosa, L. Castiglioni, M. Cimino, N. Rizzi, G. Pepe, F. Lolli, E. Marcello, L. Sironi, E. Vegeto, A. Maggi, Sex-specific features of microglia from adult mice, Cell Rep. 23 (12) (2018) 3501–3511.
[37] U.S. Food & Drug Administration, Drug Approval Package, Pharmacology Review(s), Retrieved from http://www.accessdata.fda.gov/drugsatfda_docs/nda/2002/21409_Singulair_Pharmr.pdf, 2002.
[38] M. Fisher, G. Feuerstein, D.W. Howells, P.D. Hurn, T.A. Kent, S.I. Savitz, E.H. Lo, S. Group, Update of the stroke therapy academic industry roundtable preclinical recommendations, Stroke 40 (6) (2009) 2244–2250.
[39] J. Zhang, M.V. Jones, M.T. McMahon, S. Mori, P.A. Calabresi, In vivo and ex vivo diffusion tensor imaging of cuprizone-induced demyelination in the mouse corpus callosum, Magn. Reson. Med. 67 (3) (2012) 750–759.
[40] E.R. Zanier, F. Pischiutta, P. Villa, A. Paladini, M. Montinaro, E. Micotti, A. Orru, L. Cervo, M.G. De Simoni, Six-month ischemic mice show sensorimotor and cognitive deficits associated with brain atrophy and axonal disorganization, CNS Neurosci. Ther. 19 (9) (2013) 695–704.
[41] C.H. Sotak, The role of diffusion tensor imaging in the evaluation of ischemic brain injury—a review, NMR Biomed. 15 (7–8) (2002) 561–569.
[42] N. Miyamoto, R. Tanaka, H. Shimura, T. Watanabe, H. Mori, M. Onodera, H. Mochizuki, N. Hattori, T. Urabe, Phosphodiesterase III inhibition promotes differentiation and survival of oligodendrocyte progenitors and enhances regeneration of ischemic white matter lesions in the adult mammalian brain, J. Cereb. Blood Flow. Metab. 30 (2) (2010) 299–310.
[43] L. Han, W. Cai, L. Mao, J. Liu, P. Li, R.K. Leak, Y. Xu, X. Hu, J. Chen, Rosiglitazone promotes white matter integrity and long-term functional recovery after focal cerebral ischemia, Stroke 46 (9) (2015) 2628–2636.
[44] R. Zhang, M. Chopp, Z.G. Zhang, Oligodendrogenesis after cerebral ischemia, Front. Cell. Neurosci. 7 (2013) 201.
[45] M. Chu, X. Hu, S. Lu, Y. Gan, P. Li, Y. Guo, J. Zhang, J. Chen, Y. Gao, Focal cerebral ischemia activates neurovascular restorative dynamics in mouse brain, Front. Biosci. (Elite Ed.) 4 (2012) 1926–1936.
[46] V.E. Miron, A. Boyd, J.W. Zhao, T.J. Yuen, J.M. Ruckh, J.L. Shadrach, P. van Wijngaarden, A.J. Wagers, A. Williams, R.J.M. Franklin, C. Ffrench-Constant, M2 microglia and macrophages drive oligodendrocyte differentiation during CNS remyelination, Nat. Neurosci. 16 (9) (2013) 1211–1218.
[47] D. Diaz-Lucena, M. Gutierrez-Mecinas, B. Moreno, J.L. Martinez-Sanchez, P. Pifarre, A. Garcia, Mechanisms involved in the remyelinating effect of sildenafil, J. Neuroimmune Pharmacol. 13 (1) (2018) 6–23.
[48] X. Liu, S. Wen, F. Yan, K. Liu, L. Liu, L. Wang, S. Zhao, X. Ji, Salidroside provides neuroprotection by modulating microglial polarization after cerebral ischemia, J. Neuroinflammation 15 (1) (2018) 39.
[49] P. Gelosa, F. Colazzo, E. Tremoli, L. Sironi, L. Castiglioni, Cysteinyl leukotrienes as potential pharmacological targets for cerebral diseases, Mediators Inflamm. 2017 (2017) 3454212.
[50] M.H. Muz, F. Deveci, Y. Bulut, N. Ilhan, H. Yekeler, T. Turgut, The effects of low dose leukotriene receptor antagonist therapy on airway remodeling and cysteinyl leukotriene expression in a mouse asthma model, Exp. Mol. Med. 38 (2) (2006) 109–118.